

Side-wall spacer passivated sub- μm Josephson junction fabrication process

Leif Grönberg, Mikko Kiviranta, Visa Vesterinen, Janne Lehtinen, Slawomir Simbierowicz, Juho Luomahaara, Mika Prunnila, and Juha Hassel

VTT Technical Research Centre of Finland, Tietotie 3, FI-02150 Espoo, Finland

E-mail: Juha.Hassel@vtt.fi

June 2017

Abstract. We present a structure and a fabrication method for superconducting tunnel junctions down to the dimensions of 200 nm using i-line UV lithography. The key element is a side-wall-passivating spacer structure (SWAPS) which is shaped for smooth crossline contacting and low parasitic capacitance. The SWAPS structure enables formation of junctions with dimensions at or below the lithography-limited linewidth. An additional benefit is avoiding the excessive use of amorphous dielectric materials which is favorable in sub-Kelvin microwave applications often plagued by nonlinear and lossy dielectrics. We apply the structure to niobium trilayer junctions, and provide characterization results yielding evidence on wafer-scale scalability, and critical current density tuning in the range of 0.1 – 3.0 kA/cm². We discuss the applicability of the junction process in the context of different applications, such as, SQUID magnetometers and Josephson parametric amplifiers.

1. Introduction

Superconducting tunnel junctions form the basis of many applications in the field of low-temperature sensors and electronics. A multitude of different process versions has been introduced in the past decades optimized for different applications [1, 2, 3, 4]. The starting point of this work is our established fabrication line based on niobium trilayer junctions [5, 6] that has been extensively utilised in different applications and academic explorations such as biomagnetism [7], astronomical imaging applications [8], Josephson microwave amplifiers [9], and demonstrators of parametric quantum effects [10], to mention a few. In this paper we present a modified scheme for junction patterning based on a smooth side-wall-passivating spacer structure (SWAPS) enabling an accurate definition of the junction by a self-aligned cross-type structure. Similar spacers have been previously used in other applications [11]. To our knowledge such spacers have not been used in the context of superconducting junctions while we have used a similar technique to assist step-coverage in superconductive cross-overs [6] (marked

proprietary). Cross-type superconducting junctions have been previously introduced by others [3, 12, 13]: a common aspect is that such processes enable, for a given lithography resolution, minimal junction size and very small parasitic capacitance. For our process, we present characterization data verifying that junctions with dimensions down to $0.2\ \mu\text{m} \times 0.2\ \mu\text{m}$ can be reliably produced with the process based on 150 mm wafers and UV optical lithography.

In addition to minimizing the junction size and parasitic capacitance, our approach aims at solving another issue of significance especially in sub-Kelvin applications utilizing microwave-resonant structures. It is a well-known feature of common amorphous dielectric materials that they possess excess microwave loss as well as power and temperature nonlinearity attributed to the two-level states (TLSs) present in the material [14]. This is typically considered in the context of decoherence mechanisms in quantum bits. We have found that the effects are also harmful within Josephson parametric amplifiers (JPAs), especially thanks to the temperature dependence of the real part of the dielectric constant [9]. These problems are not strictly due to the capacitances of the junctions themselves, but relate to the parasitic effect caused by the dielectric material that overall couples to the microwave resonant features of the device. For this reason, in our junction definition scheme unlike in cross-layer processes based on planarization, the dielectric materials are removed from the device area excluding the junction sidewall itself.

2. Fabrication techniques and samples

The process steps are illustrated in Figure 1. The basis of the structure is the trilayer (Fig. 1a) that is formed in a standard fashion by sputtering the base Nb layer, and on top of that a thin ($\sim 10\ \text{nm}$) Al layer [16]. Aluminium surface is then oxidized by letting oxygen into the chamber. The tunnel resistance/critical current density is determined by the oxygen exposure [17, 18]. The counter electrode Nb is sputtered on top of AlO_x . This is all done in situ without breaking the vacuum. The trilayer is patterned by i-line UV projection lithography, and plasma etched to form a strip (Fig. 1(b)). On top of this, a layer of silicon dioxide (SiO_2) is deposited by plasma enhanced chemical vapor deposition (PECVD) (Fig. 1(c)). The critical step is then to perform an anisotropic plasma etch of SiO_2 to form the SWAPS structure (Fig. 1(d)). This etch step could be replaced with techniques such as chemical-mechanical planarization [15], or liftoff-based planarization [3], the drawback of which as compared to SWAPS is that the dielectrics are left essentially everywhere in the device area. Finally, the wiring Nb layer is deposited on top, patterned by projection lithography, and plasma etched to strip geometry (Fig. 1(e,f)). The top view of the cross junction is shown in Fig. 1(g).

Scanning electron micrographs of SWAPS structures are shown in Fig. 2. In Fig. 2(a) the structure on a non-oxidized silicon wafer clearly shows the triangular cross-sectional shape in which the spacer tends to form. Figure 2(b) shows the structure applied onto a niobium trilayer, i.e. representing a realization of the structure in Fig.

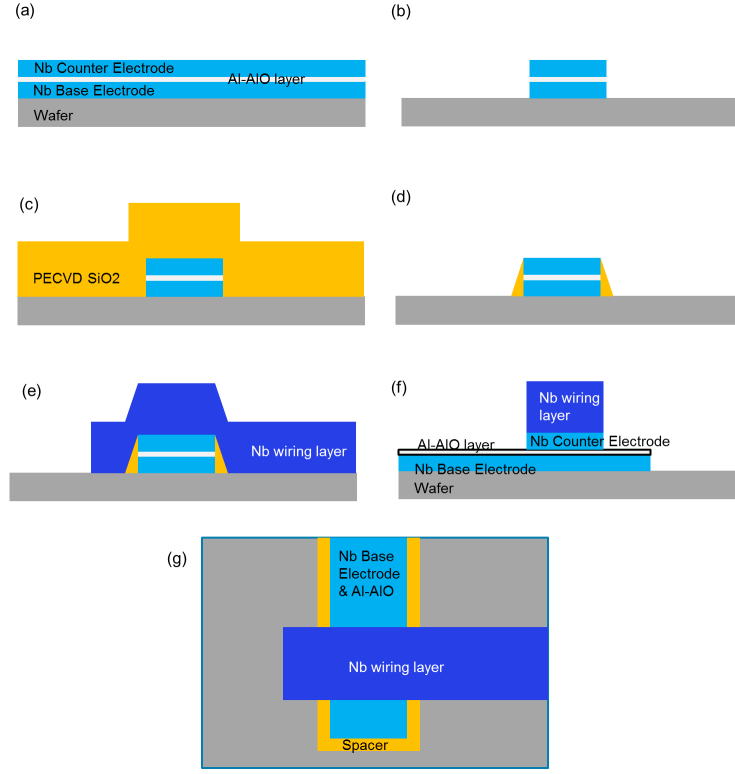


Figure 1. Illustration of the main process steps in the junction formation. (a) Trilayer deposited and oxidized. (b) Trilayer patterned. (c) Spacer material (PECVD SiO_2) deposited. (d) Spacer formed after blanko SiO_2 etch. (e,f) Wiring layer deposited and patterned. The view in (f) is 90 degrees rotated. (g) Top view of the final junction structure. The junction is formed at the area of the crossing.

1(e).

We note that on top of the junction scheme described above we have up to date developed process versions for two applications, namely SQUID magnetometers and Josephson parametric amplifiers. The versions differ from each other in terms of substrate quality (thermally oxidized/non-oxidized, respectively), and in terms of additional layers for superconducting crossings, flux input coupling, and resistive shunts. While the main emphasis here is to verify the functionality of the junction process, the data shown below is from three different wafers fabricated either just for junction testing (wafer A) or for SQUID magnetometry (wafers B,C). For wafers B,C we thus have data from resistively shunted SQUID structures as well. From the junction point of view the wafers differ from each other mainly in terms of oxygen exposure E used in the tunnel barrier formation. For wafers A,B,C it applies $E \approx 1.3 \text{ kPa-s}$, 3.5 kPa-s and, 1600 kPa-s , respectively.

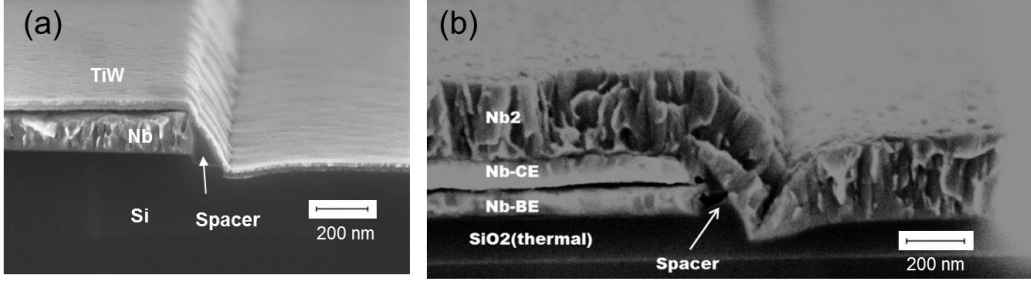


Figure 2. Scanning electron micrographs of SWAPS structures with a) plain Nb electrode on non-oxidized silicon wafer with titaniumtungsten (TiW) used for contrast enhancement and b) complete Nb trilayer junction on thermally oxidized silicon.

3. Electrical characteristics

Room-temperature tunnel resistance data from the three wafers is presented in Fig. 3. For each wafer, the resistance measurement is performed on chips with on-wafer locations as indicated in Fig. 3(a). From each chip on wafer A we have measured junctions with 20 different sizes and 3 junctions per size, i.e. altogether 60 junctions per chip and 360 junctions per wafer. From wafers B and C we have measured junctions with 18 different sizes per chip and 1 junction per size, i.e., altogether 162 junctions per wafer. The resistance data as the function of the junction dimension are presented in Fig. 3(b). The x-axis represents the dimension of the rectangular junction including the size reduction due to the lithography and overetching. The size reduction for each wafer is obtained from the fitted tunnel conductance data. For wafers A,B,C the average size reductions over wafer are $(0.29 \pm 0.02) \mu\text{m}$, $(0.52 \pm 0.01) \mu\text{m}$, and $(0.49 \pm 0.02) \mu\text{m}$, respectively. The difference between wafer A and wafers B,C may be related to the difference in the wiring layer thickness and related overetching time which was a factor of ~ 2 longer for B,C in comparison to A. The similarity between B and C indicates good reproducibility from wafer to wafer when the etching parameters are held constant. The error bars represent the statistical standard error from the least squares fit.

It has been previously observed that room temperature resistance data well predicts

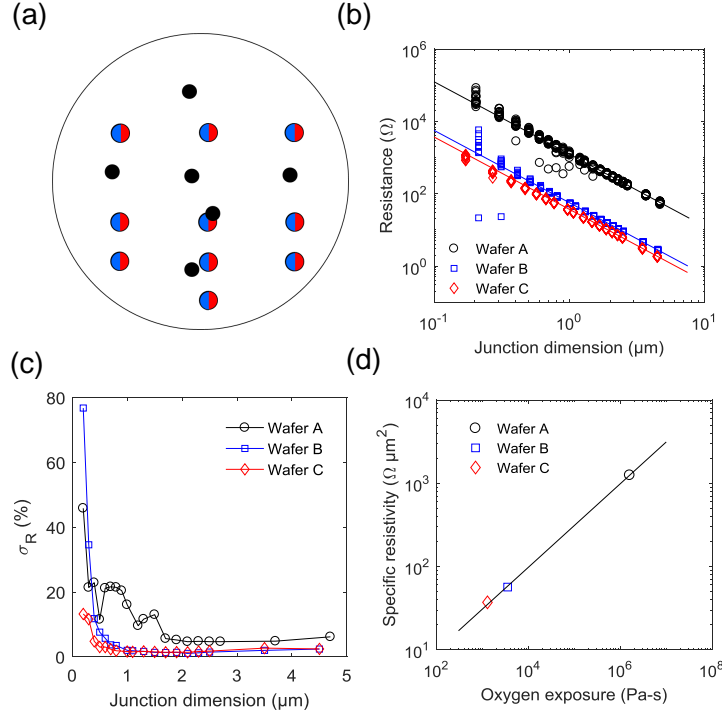


Figure 3. (a) The locations of the chips on 150 mm wafer from which the room temperature resistance data was measured: black small circles correspond to the chips of wafer A and red-blue large circles the locations on wafers B,C. (b) Junction resistance as the function of dimension. (c) Standard deviation σ_R for resistances across the wafer normalized to the median resistance of each junction size. (d) Specific tunnel junction resistivity plotted as the function of oxygen exposure. The three experimental values are obtained as fitting parameters from the data of (b), and the solid line is the power-law fit.

the low-temperature characteristics [5]. Thus it is useful to look at the statistics of the resistances that should give an indication on the expected critical current values and spread. Figure 3(c) shows the standard deviations σ_R of the junction resistances across the wafers scaled to the median value of each junction size. For wafers B,C, σ_R is below 2.5% for large junctions with dimensions $> 1 \mu\text{m}$. For wafer A the deviation is somewhat larger, $< 6\%$ for junctions down to the size of $1.7 \mu\text{m}$ and at a somewhat elevated level below this. In all wafers the deviation increases with decreasing junction size which is readily understood to be due to the increasing uncertainty of the junction dimension as the smallest junctions have the dimensions comparable to or smaller than the linewidth reduction. Yet, for all three wafers the standard deviation for junctions down to the size of $0.4 \mu\text{m}$ is below 23% across the wafer. Even the smallest junctions down to the size of approximately $0.2 \mu\text{m}$ still follow well the dimensional scaling as apparent in Fig. 3(b) though the deviation increases up to the range of 13% - 76% depending on the wafer. Furthermore, even though the spread of the smallest junctions across

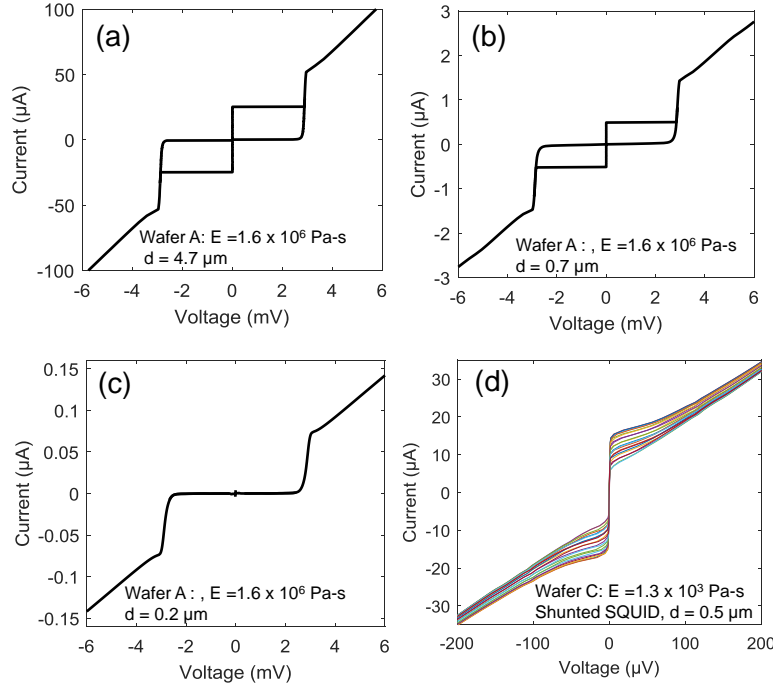


Figure 4. IV data from shunted and unshunted test structures: (a)-(c) Current-voltage characteristics of unshunted junctions from wafer A with junction dimensions indicated in the legend. (d) A family of current-voltage curves at different flux operating points from a shunted dc SQUID from wafer C. The sizes of the SQUID junctions is $0.5 \mu\text{m}$.

the wafer is relatively large, it was observed that for all junction sizes the extremal resistance difference $(\max R - \min R) / (\max R + \min R)$ within a single chip on wafer A was below 10% for a great majority of the chips. This is excluding the few individual junctions falling below the trend as apparent in Fig. 3(b).

The tunnel junction resistivity R_s is plotted as the function of oxygen exposure in Fig. 3(d). The power-law fit yields the critical exponent of 0.50 ± 0.01 . Assuming that the critical current of the junction is inversely proportional to R_s this is in line with empirical data predicting $J_c \propto E^\alpha$ with $\alpha = -0.4$ [17] or $\alpha = -0.5$ [18]. We have previously obtained an empirical prediction for the critical current density of Nb/ AlO_x junctions as $J_c = 1.22 \text{ mV}/R_s$ [5]. The resistance data thus predicts the critical current densities of $0.1 \text{ kA}/\text{cm}^2$, $2.2 \text{ kA}/\text{cm}^2$ and $3.3 \text{ kA}/\text{cm}^2$. To test the low- J_c end, Figs. 4(a)–(c) show IV curves from wafer A measured at cryostat temperatures of 10 – 15 mK. The characteristics of the quasiparticle branches of the curves verify the basic functionality of the junctions providing an energy gap of $2\Delta \approx 3.0 \text{ meV}$ as expected for Nb. The switching from the zero-voltage state yields estimated critical currents I_c of $25 \mu\text{A}$ and $0.50 \mu\text{A}$ for the junctions with nominal dimensions of $d = 4.7 \mu\text{m}$ and

0.7 μm , respectively. These are both in line within about 10% with the expected J_c . The smallest junction shows clearly suppressed critical current density with switching at about 4 nA. This is not surprising as the characteristic energy of the quantum fluctuations at the junction plasma frequency hf_p , where h is the Planck constant and f_p the plasma frequency, is in this case several times higher than the Josephson coupling energy $\Phi_0 I_c / (2\pi)$ with Φ_0 the flux quantum. To test the highest- J_c case, Fig. 4 (f) shows a set of IV curves of an externally shunted dc SQUID from wafer C at different flux operating points. The nominal dimensions of the junctions are 0.5 μm here. The recorded maximum critical current density $2I_c \approx 15 \mu\text{A}$ provides estimated critical current density of 3.0 kA/cm², i.e., within 10% from the predicted value. Thus the parameters of the junctions behave in a predictable manner across the whole J_c range.

4. Conclusions

We have presented the SWAPS structure which is effective in the precise definition of superconducting tunnel junctions. The junction characterization measurements yielded uniform junction data across the wafers indicating that the concept is functional. We verified successful lateral junction dimension scaling down to 0.2 μm and critical current density tunability in the range of 0.1 - 3 kA/cm² suggesting potential in various applications. On top of the junction process we have developed process versions optimized for SQUID magnetometers and Josephson parametric amplifiers, both of which have been up to date verified to produce functional devices. The SWAPS scheme differs from most other junction definition schemes based on optical lithography in the sense that the dielectric materials typically inherent in junction definition methods [1, 2, 3, 13] are removed from the device area. This is anticipated to be a benefit especially in sub-Kelvin applications utilizing the microwave band. In this sense our process resembles e-beam lithography and liftoff based junction definition schemes in which the junction is contacted over a smooth edge crossing [21, 22]. The SWAPS structure extends a similar approach to thicker layers and a wider range of lithography and etching techniques as verified in our case with niobium trilayers and optical lithography. Finally, we note that the SWAPS technique can also potentially be utilized in other tunnel junction applications beyond superconductive electronics. These include, for example, Coulomb blockade thermometry [23] and magnetic junctions [24]. In principle all devices where cross-line patterned functional junction can be used could benefit from SWAPS as the method is not limited to the Nb tri-layer junction of this work.

Acknowledgement

We thank Harri Pohjonen for help with lithographic masks, and Paula Holmlund for assistance in sample preparation. This work has received funding from the Academy of

Finland through grants 287768 and 284594, and through the European Unions Horizon 2020 research and innovation programme under grant agreement No 686865.

References

- [1] Tolpygo K T, and Amparo D 2010 *Supercond. Sci. Technol.* **23**(3) 034024
- [2] Nagasawa S, Satoh T, Hinode K, Kitagawa Y, Hidaka M, Akaike H, Fujimaki A, Takagi K, and Yoshikawa N 2009 *Phys. C* **469** 1578
- [3] Anders S, Schmelz M, Fritzsche L, Stolz R, Zakosarenko V, Schönau T, Meyer H-G 2009 *Supercond. Sci. Technol.* **22**(6) 064012
- [4] Muller F, Schulze H, Behr R, Kohlmann J, and Niemeyer J 2001 *Phys. C* **354**(1-4) 66
- [5] Grönberg L, Hassel J, Helistö P, and Ylilammi M, 2007 *IEEE Trans. Appl. Supercond.*, **17**(2) 952
- [6] Kiviranta M, Brandel O, Grönberg L, Künert J, Linzen S, Beev N, May T, and Prunnila M 2016 *IEEE Trans. Appl. Supercond.*, **26**(6) 7438771
- [7] Vesanen P T, Nieminen J O, Zevenhoven K C J, Dabek J, Parkkonen L T, Zhdanov A V, Luomahaara J, Hassel J, Penttilä J, Simola J, Ahonen A I, Mäkelä J, and Ilmoniemi R J 2013, *Magn. Reson. Med.* **69**(6) 1795
- [8] Gottardi L, Kiviranta M, van der Kuur J, Akamatsu H, Bruijn M P, and den Hartog R 0214, *IEEE Trans. Appl. Supercond.* **25**(3) 2100404
- [9] Vesterinen V, Saira O-P, Räisänen I Möttönen M, Grönberg L, Pekola J, and Hassel J 2017 *Supercond Sci. Technol.*, in print
- [10] Lähteenmaki P, Paraoanu G S, Hassel J, and Hakonen P J 2016 *Nature Commun.* **7**(11) 12548
- [11] Franssila S. 2004, *Introduction to Microfabrication*, John Wiley and Sons Ltd.
- [12] Aoyagi M, Shoji A, Kosaka S, Shinoki F, Hayakawa H, in *Adv. Cryog. Engin. Mater.* 1986 **62**, Eds. R. P. Reed, and A. F. Clark, Plenum Publishing Corporation.
- [13] Dang H, and Radparvar M 1991 *IEEE Trans. Magn.* **27**(2) 3157
- [14] Martinis J M, Cooper K B, McDermott R, Steffen M, Ansmann M, Osborn K D, Cicak K, Seongshik Oh, Pappas D P, Simmonds R W, and Yu C C 2005 *Phys. Rev. Lett.* **95** 210503
- [15] Ketchen M B et al. 1991 *Appl. Phys. Lett.* **59**(20) 2609
- [16] Gurvitch M, Washington M A, and Huggins H A 1982 *Appl. Phys. Lett.* **42**(5) 472
- [17] Kleinsasser A W, Miller R E, and Mallison W H 1995 *IEEE Trans. Appl. Supercond.* **5**(1) 26
- [18] Sugiyama, Fujimaki A, and Hayakawa H 1995 *IEEE Trans. Appl. Supercond.* **5**(2) 2739
- [19] Tesche C D, and Clarke J 1977 *J Low Temp. Phys.* **29**(3) 1977
- [20] Schmelz M, Zakosarenko V, Schnau T, Anders S, Kunert J, Meyer M, Meyer H-G, and Stolz 2017 *Supercond. Sci. Technol.* **30**(7) 074011
- [21] Pop I M, Fournier T, Crozes T, Lecocq F, Matei I, Pannetier B, Buisson O, Guichard W 2012 *J Vac. Sci. Technol. B* **30**(1) 010607
- [22] Wu X, Long H, Ku H S, Lake R E, Bal M, Pappas D P 2017, arXiv:1705.08993
- [23] Pekola J P, Hirvi K P, Kauppinen J P, Paalanen M A 1994 *Phys. Rev. Lett.* **73** 2903
- [24] Otani Y, Kubota H, Fukushima A, Maehara H, Osada T, Yuasa S, and Ando K, *IEEE Trans. Magn.* 2007 **43** (6) 2776